Research On Secondary Control Strategy Of Microgrid Based On Adaptive Virtual Impedance

Baoge Zhang, Xiong Lv*, Hao Tian, Yongquan Ren, and Fuhong Cui

School of Automation and Electrical Engineering, Lanzhou Jiaotong University, Lanzhou,730070, China

Corresponding author. E-mail: 2306336310@qq.com

Received: July 22, 2023; Accepted: Dec. 18, 2023

Distributed power sources are generally connected to the microgrid through inverters. However, due to the output line impedance mismatch, it will result in the traditional droop control not being able to achieve accurate reactive power sharing. To address this problem, this paper proposes an improved droop control strategy based on virtual impedance. The output reactive power mismatch term is introduced into the droop control as a feedback signal to achieve the adaptive adjustment of virtual impedance and improve the accuracy of reactive power sharing. Meanwhile, the adaptive regulation strategy of secondary frequency and voltage recovery is proposed. The frequency offset and voltage offset during the stable operation of the system are compensated. Finally, the three inverters parallel system of isolated microgrid is built in matlab/Simulink for simulation study. The reactive power output of the parallel system without adaptive virtual impedance is compared to the reactive power output of the parallel system without adaptive virtual impedance ($Q_1 = 3000$var, $Q_2 = 2000$var, $Q_3 = 1000$var) in $0 - 2$ s. The output reactive power of the parallel system with the addition of the adaptive virtual impedance is $Q_1 = Q_2 = Q_3 = 2000$ var. the addition of the virtual impedance achieves good power equalization. At the same time, the secondary voltage and frequency strategies are added so that the output voltage and frequency of the parallel system after adding the adaptive virtual impedance are restored to 311 V and 50 Hz from the original 310 V and 49.7 Hz. The frequency and voltage offsets are compensated. The simulation results verify the effectiveness and feasibility of the proposed control strategy.

Keywords: droop control, virtual impedance, frequency offset, voltage offset

http://dx.doi.org/10.6180/jase.202501_28(1).0005

1. Introduction

With the rapid development of the national economy and the massive popularity of the concept of green energy. It has increased people's attention to renewable energy, and also increased the penetration rate of renewable energy in the power grid. It makes distributed generation technology gradually enter the modern energy field [1–3]. Microgrids are small-scale grids formed by distributed power sources and loads, and are also an effective way of integrating renewable energy sources. Microgrids can work in both on-grid and off-grid operation modes, which enhances grid flexibility and reliability. It also improves power quality and user availability [4–6]. when the microg-rid operates on-grid. The main grid provides frequency and voltage reference values for the microgrid and exchanges power with the microgrid through contact lines. In contrast. In the off-grid state, system frequency and voltage stability are maintained by the microgrid itself. And it is necessary to maintain the balance of supply and demand between the microgrid and the users at all times. Otherwise, it will cause the system frequency and voltage to deviate from their rated values, making the system up to unstable operation.

Droop control that mimics the idea of synchronous generators has the advantages of eliminating the need for communication interconnection lines and high reliability. It becomes the main control method of isolated microgrid inverter. Droop control has the function of regulating the DC microgrid voltage while satisfying the balanced power distribution of each DG. Therefore, droop control has been widely adopted in microgrids. For example. In the literature [7], an improved droop control strategy with secondary regulation is proposed. An indirect equalization method is used to distribute the load current of the shunt alternator based on the shunt-type staggered voltage balancing. In the literature [8], the problem of not being able to reasonably allocate the capacity due to different line impedances is addressed. An improved droop control strategy is proposed. The virtual negative impedance is used to compensate for the difference between line impedances, and the proportionally accurate equal distribution of power is accomplished. In the literature [9], a self-tuning controller based on reliable sag coefficient is proposed. When the transmission line changes, the reasonable sharing of power among inverters is achieved by adjusting the parameters of the controller. The system frequency is maintained constant at the same time. The stability of system operation is improved. In practical applications, P-f and Q-V droop control methods should be used when the line reactance is much larger than the resistance. P-V and Q-f control should be selected when the line resistance is much larger than the reactance [10]. However, due to line impedance mismatch and frequent load casting and cutting, the reactive power cannot be reasonably balanced. It leads to the reduction of system stability. Therefore, how to adopt a more reasonable droop control is the primary problem solving nowadays [11]. In order to compensate for the frequency and voltage offset caused by the traditional droop control. Secondary coordinated control needs to be introduced to compensate for the voltage and frequency offset, so that the frequency and voltage are synchronous with the original set values. Improving the power quality of the microgrid.

Secondary coordinated control is mainly applied in the important area of microgrid voltage and frequency offsets. The corresponding voltage and frequency adjustments are obtained with the help of the output frequency and output voltage between each DG. The adjustment amount is fed back to the conventional droop control for compensation so that the output voltage and frequency are approximated to the rated values. The system is restored to a stable operating state. Secondary coordinated control is subdivided into centralised and distributed control methods [12, 13]. The more traditional centralised control method uses the microgrid central processor to detect the system corner frequency and voltage. The primary control reference is then set by PI control. Although it has the advantages of fast response and rapid system convergence, it still has the shortcomings of cumbersome communication and poor robustness. And for real-time and reliability requirements are high, the slightest error will cause very serious consequences. On the contrary, the distributed control method does not need a central processor to collect information. Only need to complete the information exchange between nearby controllers. And the response speed can be improved by processing data in parallel [14].

Scholars have proposed a variety of control methods to address the problem of microgrids' inability to reasonably distribute power in a balanced manner. In the literature [15], a method is proposed by changing the droop curve. The method of dynamically adjusting the droop coefficient is used to achieve accurate distribution of reactive power. However, too large droop coefficients lead to large deviations in the system output voltage, which reduces the stability of the microgrid system. In the literature [16], an improved droop control based on virtual negative resistance is proposed. The virtual negative resistance is used to offset the resistive part of the line and improve the inductive resistance of the inverter output impedance. Reasonable equal distribution of output power of each inverter is achieved. And the accuracy of power distribution is improved. However, it also reduces the output voltage and the stability of the system. For the problem of voltage and frequency shifts caused by the described power equalization. In the literature [17], an improved adaptive sectional sag control method is proposed. While improving the power allocation accuracy, it also improves the bus voltage excursion rate. The stability of the system operation is improved. In literature [18], the concept of voltage correction parameter is proposed in droop control. The correction parameter is adjusted by feeding back the current of each DG. The voltage offset is reduced. In the literature [19], an improved droop control strategy based on adaptive virtual impedance is proposed. While the power is reasonably evenly divided, a voltage compensation link is introduced. The deviation of the output voltage from the rated voltage is eliminated.

On the basis of existing research. In order to solve the problem that the power cannot be reasonably divided equally and the voltage and frequency shifts due to different line impedances. In comparison with the traditional droop control, this paper presents a study of a microgrid secondary control strategy based on adaptive virtual impedance. The significant contributions of the proposed

work are set out below:

1. In contrast to the two inverters study. The adaptive virtual impedance based secondary control strategy for microgrids proposed in this paper is applicable to three and more inverter operations. It increases the number of inverters working. Meeting the needs of a wider range of customers.

2. The adaptive virtual impedance control strategy proposed in this paper communicates through its own DG information and neighbour information. It generates adaptive virtual impedance and thus compensates the difference between line impedances. The problem of the difficulty of measuring impedance online is solved. It compensates the line impedance in real time and achieves the accurate sharing of power.

3. The secondary control strategy proposed in this paper. The output voltage and frequency are used to obtain the corresponding trimming amount, which is fed back to the primary control for frequency and voltage compensation. So that there is no frequency and voltage offset in steady state. The voltage-frequency dips caused by the droop control and the introduction of virtual impedance are solved. Improving the power quality of the microgrid.

4. The proposed control strategy is compared with the conventional droop control strategy. And the effectiveness of the proposed control strategy is verified by simulation in matlab/Simulink.

2. Traditional droop control strategy

Fig. 1 shows the distributed structure of the microgrid in islanding mode. It consists of distributed power supply (DG), LC filter, line impedance and control structure. Among them, the control part includes power calculation, droop control, voltage and current double closed loop, and secondary control. In the Figure 1, u_{od} and u_{oq} are the d-axis and q-axis components of the capacitive voltage u_{oabc} after coordinate transformation. i_{od} and i_{oq} are the d-axis and q-axis components of the capacitive current i_{oabc} after coordinate transformation. i_{Ld} and i_{Lq} are the d-axis and q-axis components of the inductive current i_{Labc} after coordinate transformation. P_i and Q_i are the inverter output active and reactive power, respectively. ω_0 and u_0 are the rated angular frequency and rated voltage amplitude, respectively. u_{dref} and u_{qref} are the d-axis and q-axis components of the input voltage after droop control. i^*_{Ld} and i^*_{Lq} are the output currents after voltage loop control, as the given values of the current loop. u^*_d and u^*_q are the current loop output voltage values, which are used as the given values for the SPWM controller. $\Delta\omega_i$ and Δu_i are the secondary control angle frequency and voltage reference values.

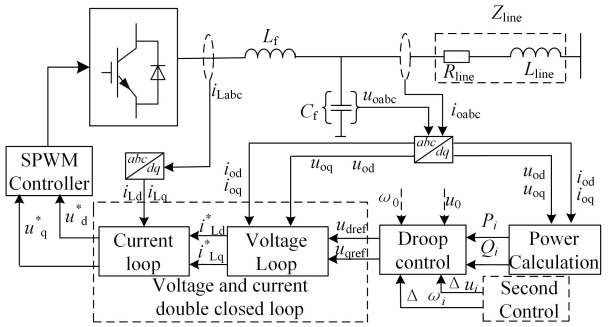

Fig. 1. Microgrid distributed control structure

Droop control enables the DG units to work independently in islanded operation mode, enabling "plug-and-play" operation without the need to communicate with each other. The simplified model of inverter parallel connection is shown in Fig. 2. where $U_i\angle\phi_i$ and Z_i are the output voltage and equivalent output impedance of the microsource, respectively. Z_L is the load impedance. $U_p\angle 0^\circ$ is the bus voltage at the common point.

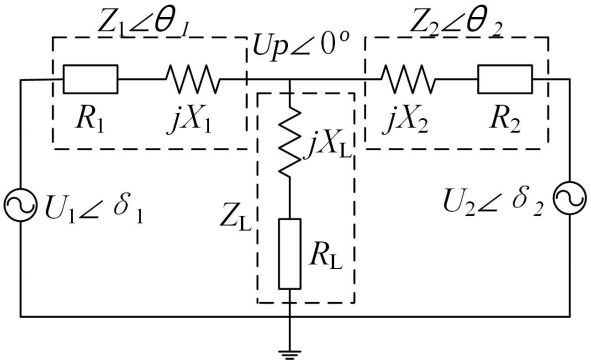

Fig. 2. Simplified diagram of inverter parallel connection

When the DG unit is connected to the common AC bus through the line impedance. the active and reactive power injected into the bus by the DG can be expressed as

$$\begin{cases} P_i = \frac{U_iU_P\cos\delta_i - U_P{}^2}{Z_i}\cos\theta_i + \frac{U_iU_P}{Z_i}\sin\delta_i\sin\theta_i \\ Q_i = \frac{U_iU_P\cos\delta_i - U_P{}^2}{Z_i}\sin\theta_i - \frac{U_iU_P}{Z_i}\sin\delta_i\cos\theta_i \end{cases} \quad (1)$$

Then bring the line impedance $Z_ie^{j\theta_i} = R_i + jX_i$ into the Eq. (1) can be obtained

$$\begin{cases} P_i = \frac{U_i}{R_i^2+X_i^2}\left[R_i\left(U_i - U_p\cos\delta_i\right) + X_i U_P \sin\delta_i\right] \\ Q_i = \frac{U_p}{R_i^2+X_i^2}\left[X_i\left(U_i - U_p\cos\delta_i\right) - R_i U_i \sin\delta_i\right] \end{cases} \tag{2}$$

In Eqs. (1) and (2), U_p is the common point bus voltage amplitude. U_i is the microsource DG output voltage amplitude. δ_i is the power angle between U_i and U_p.Z_i and θ_i are the impedance value and phase corresponding to the line impedance, respectively.

The equivalent output impedance in the actual low-voltage microgrid system is resistive. There is severe coupling of the inverter output power, which will cause the droop control to be unusable. However, some micro sources need to be boosted by a transformer to meet the working requirements in practice. And the distributed power supplies are generally connected to the system through LC filters. Therefore the presence of filters and transformers makes the equivalent output impedance of the distributed power supply approximately inductive, which facilitates the use of droop control [20]. In this paper, the equivalent output impedance is studied analytically as an example of inductance. And considering that δ_i is generally small, an approximation can be made and considered $\sin\delta_i = \delta_i, \cos\delta_i \approx \delta_i$ [21, 22]. Then the microgrid output power expression can be simplified as

$$\begin{cases} P_i = \frac{U_i \cdot U_p \delta_i}{X_i} \\ Q_i = \frac{U_p\left(U_i - U_p\right)}{X_i} \end{cases} \tag{3}$$

From Eq. (3), it can be obtained that the active power is strongly dependent on the power angle δ_i. The reactive power is mainly influenced by the voltage magnitude difference. Therefore, the droop control can be expressed as [23]

$$\omega_i = \omega_0 - m_i P_i \tag{4}$$

$$U_i = U_0 - n_i Q_i \tag{5}$$

In Eqs. (4) and (5), ω_0 and U_0 are the angular frequency and amplitude of the output voltage at no-load condition. m_i and n_i are the frequency and voltage droop coefficients of DG. The resistive component in the line impedance is high in the low-voltage microgrid, which leads to a strong coupling between the system output power and reduces the system stability. Therefore, the traditional droop control does not meet the system requirements, so it is necessary to add virtual inductors to the droop control to make the line inductive in the end. The power is decoupled to meet the user requirements as much as possible.

3. Power analysis and graph theory

3.1. Power Analysis

In the operation and control process of microgrid. When multiple distributed power sources act together on the load, the active power is realized by P-f droop control. When the system enters the steady state, the frequency is homogeneous in the whole network. Therefore, each droop factor is set according to Eq. (4) to satisfy Eq. (6). So that the active power can be reasonably distributed. The active power and active droop factor are inversely proportional to each other.

$$\begin{cases} \omega_1 = \omega_2 = \ldots = \omega_n \\ m_1 P_1 = m_2 P_2 = \ldots = m_n P_n \end{cases} \tag{6}$$

In the microgrid operation and control. The reactive power is mainly realized by Q-U droop control. In order to enable the reactive power to be distributed proportionally, the corresponding reactive power droop factor is inversely related to the reactive power.

$$n_1 Q_1 = n_2 Q_2 = \ldots = n_N Q_N \tag{7}$$

According to the analysis of traditional droop control and inverter output power. Bringing Eq. (5) into Eq. (3) yields the reactive power expression as

$$n_i Q_i = \frac{U_p\left(U_0 - U_p\right)}{\frac{X_i}{n_i} + U_P} \tag{8}$$

Combining Eqs. (7) and (8) yields

$$\frac{X_1}{n_1} = \frac{X_2}{n_2} = \frac{X_3}{n_3} = \ldots = \frac{X_N}{n_N} \tag{9}$$

From Eq. (9), the droop factor and line impedance must vary proportionally if a reasonable equalization of reactive power output is to be achieved. At the same time, under the joint action of Eq. (7). The line reactance and reactive power must be inversely related. Therefore, to solve the problem that the reactive power cannot be reasonably equalized due to different impedances. The virtual electric induction is designed according to the configuration principle of Eq. (10) [24].

$$\frac{X_1}{X_2} = \frac{n_1}{n_2} = \frac{Q_2}{Q_1} \tag{10}$$

Due to the inability to achieve mutual matching between each DG line impedance, the conventional droop control cannot achieve accurate distribution of reactive power. Therefore, in actual practice, a sufficiently large virtual reactance value $(Xv >> Rv + jXv)$ is generally added to match different line impedances to achieve power decoupling control.

$$X_{v,i} = X^*_{v,i} + \Delta X_{v,i} \tag{11}$$

In Eq. (11), $X_{v,i}$ is the equivalent virtual reactance value implemented by the DG controller. $X^*_{v,i}$ is the static virtual reactance that ensures that the line becomes inductive. $\Delta X_{v,i}$ is the adaptive virtual reactance for accurate reactive power distribution. The equivalent output impedance of the line after the introduction of the virtual reactance is expressed as

$$X_i = X_{\text{line},i} + X_{v,i} \tag{12}$$

In Eq. (12), $X_{\text{line},i}$ is the output line impedance value of each DG. With the action of Eqs. (10) to (12). The relationship between line impedance, virtual impedance and power when multiple inverters are connected in parallel can be derived as

$$\begin{aligned}&\left(X_{\text{line},1} + X^*_{v,1} + \Delta X_{v,1}\right) Q_1 = \left(X_{\text{line},2} + X^*_{v,2} + \Delta X_{v,2}\right) Q_2 \\ &= \ldots = \left(X_{\text{line},N} + X^*_{v,N} + \Delta X_{v,N}\right) Q_N\end{aligned} \tag{13}$$

In the Eq. (13), the line impedance $X_{\text{line},1} \neq X_{\text{line},2} \neq \ldots X_{\text{line},N}$ is not the same. By the adaptive compensation of $\Delta X_{v,i}$, the adaptive virtual reactance is made to compensate for the effects due to different line impedances. The reactive power can be precisely and reasonably shared among DGs.

Adding a virtual inductor to the system allows for accurate reactive power sharing. However, it also increases the total impedance of the line, causing voltage dips. The voltage dip at the output of the system becomes more severe as the added inductance increases.

$$U^*_{\text{ref}} = U_{\text{ref}} - X_{v,i} i_{\text{od}} \tag{14}$$

In Eq. (14), U^* ref is the output voltage reference after adding the virtual inductor. U_{ref} is the voltage reference value of the conventional droop control output. i_{od} is the output current i_{oabc} obtained after coordinate transformation of the d-axis current. From Eq. (14), it can be concluded that the original reference voltage produces a dip under the action of the virtual inductor. At the same time, it will make the system output voltage will also produce dip, affecting the power quality of the system output. Therefore, it is necessary to adopt relevant control strategies to improve the voltage dip problem.

3.2. Graph Theory

In the case of distributed control, a topological directed graph describing the topology between agents is taken for analysis. The communication topology graph is denoted by $G = (V, E, A)$. It is composed of a vertex nonempty finite set $V = \{1, 2, \ldots, N\}$, an edge set $E \in V \times V$ and an adjacency weighting matrix $A = \left[a_{ij}\right]$. If a path exists between nodes i and j, the topology graph G is called a connectivity graph. The nodes between directed graphs represent each DG agent in the microgrid. The edges denote the communication lines between DGs. where $\left(v_i, v_j\right)$ denotes the information obtained by agent i from agent j. For directed graphs, agent i can only receive information from neighbor $N = \left\{j \in N \left(v_i, v_j\right) \in E\right\}$. a_{ij} is the weight of edge $\left(v_i, v_j\right)$ if $\left(v_i, v_j\right) \in E$ then $a_{ij} = 1$ and vice versa $a_{ij} = 0$.

4. Adaptive virtual impedance control

The difference between line impedances is an important factor that prevents reasonable equalization of reactive power. Virtual impedance is a software control technique that can change the equivalent line impedance of the inverter. On the one hand, it solves the problem of line resistance component. And on the other hand, it reduces the cost and power loss. However, the line impedance changes with the environment and other factors. When multiple inverters work together, the process of measuring line impedance is more complicated and precise measurement cannot be achieved. Therefore, this paper proposes a method of adaptive virtual impedance with reactive feedback, which solves various problems such as online measurement difficulties and inaccuracies. In conclusion. The coordinated control of reactive power sharing is a regulator synchronization problem for first-order linear multi-intelligent systems [25].

$$n_i Q_i = u_{Qi} \tag{15}$$

In Eq. (15), each inverter's own information is used together with its neighboring information as an auxiliary control for reactive power mismatch.

$$u_{Qi} = -C_{nQ} e_{n_i Q_i} \tag{16}$$

In Eq. (16), C_{nQ} is the coupling gain. $e_{n_{Q,i}}$ is the reactive power sharing error.

$$e_{n_i Q_i} = \sum_{j=N_i} a_{ij} \left(n_i Q_i - n_j Q_j\right) \tag{17}$$

In Eq. (17), a_{ij} is the adjacency matrix. From Eqs. (15) to (17), the virtual impedance correction term can be obtained as shown in Eq. (18)

$$\Delta Q_i = \left(k_{L,\text{p}} + \frac{k_{L,\text{i}}}{s}\right) u_{Qi} \tag{18}$$

In Eq. (18), ΔQ_i is the virtual impedance correction term. $k_{L,\text{p}}$ and $k_{L,\text{i}}$ are the proportionality and integration coeffi-

cients used to adjust the virtual inductance correction term, respectively.

Based on the above analysis, the adaptive virtual inductor control block diagram can be obtained as shown in Fig. 3. Using each DG to communicate with each other to obtain the reactive power mismatch term. The mismatch term is passed through the proportional integration controller to generate the impedance correction term ΔQ_i. The adaptive virtual inductance is then obtained by making a difference with the static virtual reactance phase.

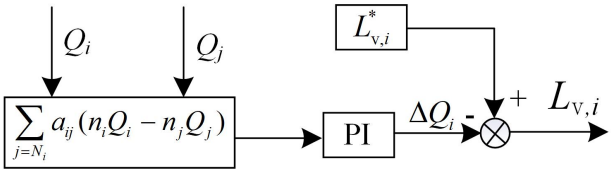

Fig. 3. Adaptive virtual impedance control block diagram

According to Fig. 3, the adaptive virtual inductor can be obtained as shown in Eq. (19). When reactive power cannot be precisely equalized, the reactive power mismatch generated by the local neighbor reactive power information is used to adaptively adjust the virtual inductor.

$$L_{v,i} = L^*_{v,i} - \Delta Q_i \tag{19}$$

In Eq. (19), $L^*_{v,i}$ is the static virtual inductance of each DG line for compensation, mainly used to ensure that the line becomes inductive. $L_{v,i}$ is the adaptive virtual inductance value. The expression of the inverter output voltage reference in the dq coordinate system after the introduction of the virtual inductance is

$$\begin{cases} U^*_{d\_ref} = U_{d\_ref} + X_v i_{oq} - \frac{X_v}{\omega}\frac{di_{od}}{dt} \\ U^*_{q\_ref} = U_{q\_ref} - X_v i_{od} - \frac{X_v}{\omega}\frac{di_{oq}}{dt} \end{cases} \tag{20}$$

In Eq. (20), $U^*_{d\_ref}$ and $U^*_{q\_ref}$ are the components of the voltage reference in the d-axis and q-axis after adding the virtual impedance. U_{d_ref} and U_{q_ref} are the components of the voltage reference in the d-axis and q-axis of the conventional droop control output. i_{od} and i_{oq} are the components of the capacitor current i_{oabc} in the d-axis and q-axis after coordinate transformation.

Fig. 4 shows the droop characteristic curves before and after the introduction of the virtual inductor. Where, Q_i and U_i are the reactive power output and voltage values of the inverter corresponding to the conventional droop. Q'_i and U'_i are the reactive power output and voltage values of the inverter after the introduction of the virtual inductor. ΔQ and $\Delta' Q$ are the reactive power difference before and after the introduction of the virtual inductor. It is observed from Fig. 4. The introduction of the virtual inductor reduces the reactive power difference between the inverters. However, it also makes the output voltage drop from U_p to U'_p, which reduces the power quality of the microgrid. Therefore, it is particularly important to compensate the voltage using secondary coordination control.

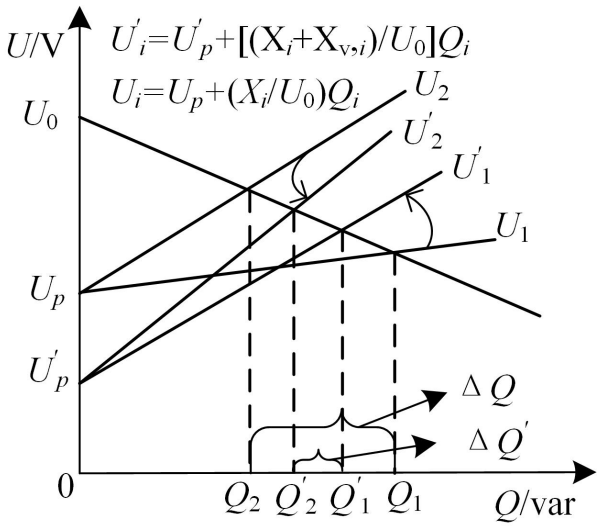

Fig. 4. Droop characteristic curve before and after the introduction of virtual inductor

5. Secondary coordinated control of microgrids

5.1. Secondary voltage control

The virtual impedance solves the power reasonable equalization while reducing the voltage amplitude. In order to compensate the voltage deviation caused by conventional droop and virtual impedance. In this paper, a secondary voltage compensation control strategy is proposed. Each DG uses its own voltage output E_i and the voltage output E_j of its neighboring DGs to obtain an estimate of the DG voltage. The microgrid output voltage is restored to within the acceptable range of the rated voltage.

$$\bar{E}_i(t) = E_i(t) + \sum_{j\in N_i} a_{ij}\left(E_j(t) - E_i(t)\right) \tag{21}$$

In Eq. (21), a_{ij} is the adjacency matrix, which is set to 1 for ease of analysis. $\bar{E}_i$ is the estimate generated by DG_i. When the estimated value of the voltage does not want to match with the microgrid reference voltage, then there is

$$u_{Ei} = U_0 - \bar{E}_i \tag{22}$$

In Eq. (22), u_{Ei} is the voltage mismatch value. In the case of mismatch, the mismatch value is passed through the

proportional-integral PI controller to generate the voltage correction term ΔU_i.

$$\Delta U_i = \left(k_{u,\mathrm{p}} + \frac{k_{u,\mathrm{i}}}{s}\right) u_{Ei} \tag{23}$$

Eq. (23), $k_{u,\mathrm{p}}$ is the proportional gain used to adjust the voltage correction term. $k_{u,\mathrm{i}}$ is the integration factor used to adjust the voltage correction term. The resulting voltage correction term is used to update the local voltage setting value to restore the voltage to the rated value. According to the above analysis, the secondary voltage recovery block diagram can be obtained as shown in Fig. 5.

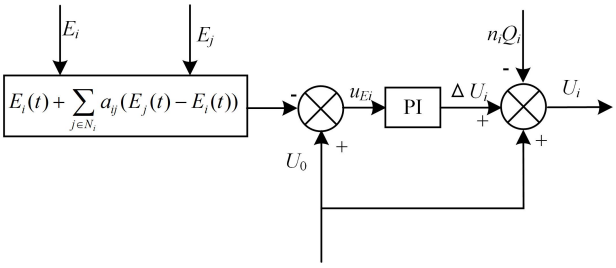

Fig. 5. Secondary voltage recovery control block diagram

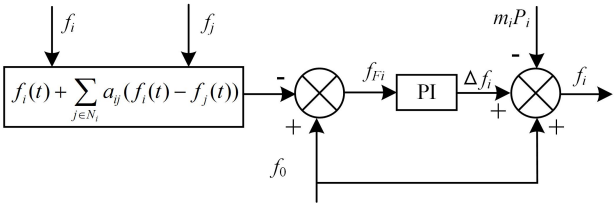

Fig. 6. Block diagram of secondary frequency recovery control

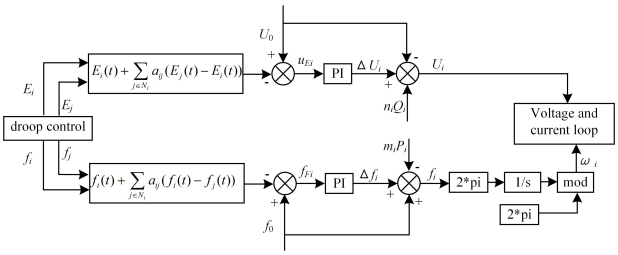

Fig. 7. System principle general control block diagram

Through the secondary voltage recovery control block diagram in Fig. 5, we can obtain the output voltage expression after adding the secondary strategy as

$$U_i = U_0 - n_i Q_i + \Delta U_i \tag{24}$$

In Eq. (24), U_i is the output voltage amplitude of each DG after secondary control. U_0 is the rated voltage value of the inverter at no load. ΔU_i is the voltage correction term. When the reactive power completes equalization, on top of the original conventional droop control. By adding the voltage correction term through the voltage secondary control, the voltage can be restored to the acceptable range of the rated value. The power quality of the grid is improved

5.2. Secondary frequency control

By conventional droop control, the system operating frequency is shifted relative to the rated frequency while achieving active power equalization. This has a non-negligible impact on the stable operation of the system. Therefore, in order to compensate for the resulting frequency deviation. In this paper, the secondary frequency recovery control strategy is also proposed successively. The corresponding frequency estimates are generated mainly by the frequency output f_i of each DG and the frequency output f_j of the neighboring DGs. In turn, the frequency correction term is obtained. It is sent to the conventional active droop control to restore the microgrid system frequency to the rated value.

$$\bar{f}_i(t) = f_i(t) + \sum_{j\in N_i} a_{ij}\left(f_i(t) - f_j(t)\right) \tag{25}$$

In Eq. (25), a_{ij} is the adjacency matrix, which is set to 1 for the convenience of analysis. $\bar{f}_i$ is the frequency estimate generated by DG_i. In actual operation, when the frequency estimate deviates from the grid frequency.

$$f_{Fi} = f_0 - \bar{f}_i \tag{26}$$

In Eq. (26), f_{Ei} is the frequency mismatch value. In order to make the frequency coupled with the grid frequency. The mismatch value is passed through the PI controller to generate the frequency correction term Δf_i.

$$\Delta f_i = \left(k_{f,\mathrm{p}} + \frac{k_{f,\mathrm{i}}}{s}\right) f_{Fi} \tag{27}$$

In Eq. (27), $k_{f,\mathrm{p}}$ is the proportional gain of the regulation frequency correction term. $k_{f,\mathrm{i}}$ is the integration factor of the regulation frequency correction term. The generated frequency correction term is mainly used to update the frequency setting value of each DG, so that the frequency offset is within the acceptable range of the grid frequency. According to the above analysis. The secondary frequency recovery block diagram can be obtained as shown in Figure 6.

According to Fig. 6, it can be obtained after adding the secondary control. The frequency recovery expression is

$$f_i = f_0 - m_i P_i + \Delta f_i \tag{28}$$

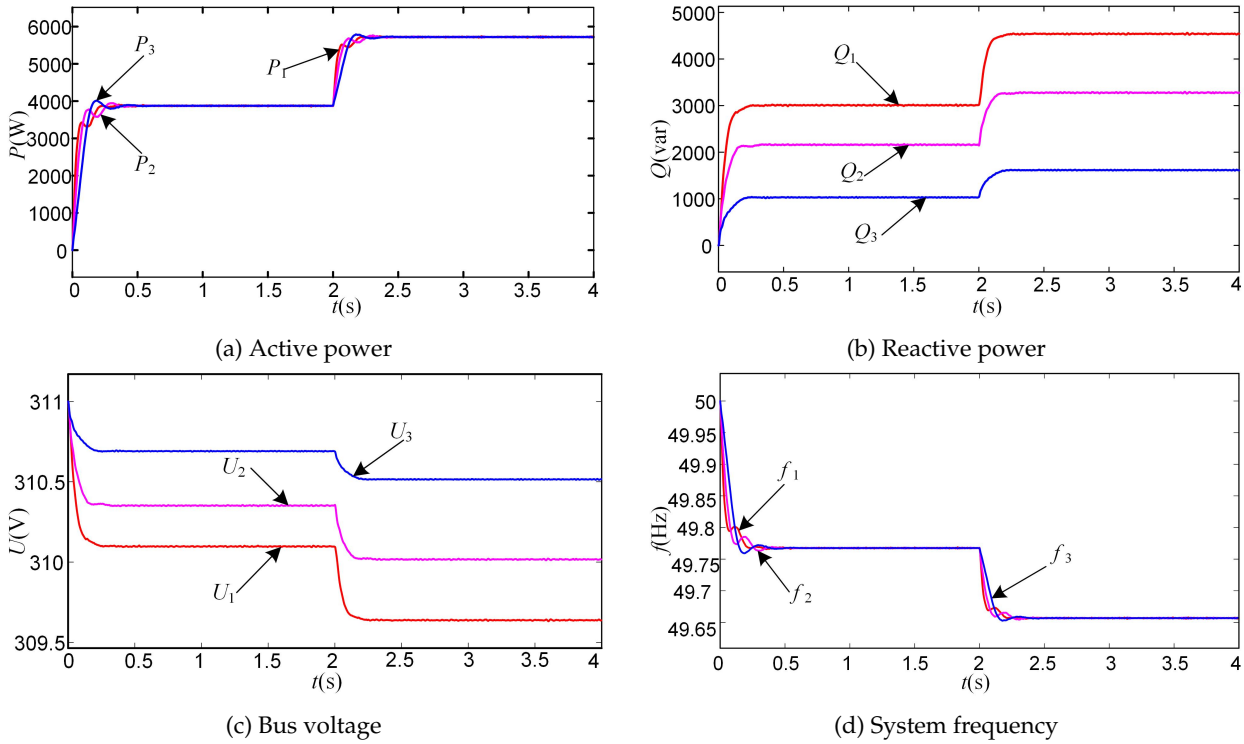

(a) Active power (b) Reactive power

(c) Bus voltage (d) System frequency

Fig. 8. Simulation results of conventional droop control

Table 1. System Simulation Parameters

Parameters/Units	Take value	Parameters/Units	Take value
U_{dc} /V	750	$L_{\mathrm{line3\,3}}$/mH	6
R_{f}/Ω	0.05	m	6e − 5
L/mH	1.5	n	3e − 4
C/μF	50	$k_{L,\mathrm{p}}$	1e − 4
$R_{\mathrm{line1\,1}}/\Omega$	0.1	$k_{L,\mathrm{i}}$	1e − 3
R_{line2} /Ω	0.1	$k_{u,\mathrm{p}}$	0.2
$R_{\mathrm{line3\,3}}/\Omega$	0.2	$k_{u,\mathrm{i}}$	20
$L_{\mathrm{line1\,1}}$/mH	2	$k_{f,\mathrm{p}}$	0.2
$L_{\mathrm{line\,2}}$/mH	3	$k_{f,\mathrm{i}}$	20

In Eq. (28), f_i is the final frequency output. f_0 is the rated frequency value of the inverter at no-load condition. Δf_i is the frequency correction term. Based on the traditional droop control, the proposed secondary frequency control strategy is used to compensate for the effect of frequency deviation. The system frequency is restored to the rated value to improve the stability of the system operation.

Fig. 7 shows the total control block diagram of the secondary system principle. The local and adjacent voltages E_i and E_j output from the conventional droop control are subjected to the proposed secondary voltage control to obtain the improved voltage output U_i. The output frequencies f_i and f_j are subjected to the proposed quadratic frequency control to obtain the improved frequencies. The resulting frequency f_i is then factored to obtain the corresponding angular frequency output ω_i. Finally, the resulting voltage U_i and ω_i are applied together in a voltage-current double closed loop.

6. Simulation analysis

The control strategy proposed in this paper has good control effectiveness and feasibility in multiple inverter systems. In this paper, Simulink simulation models are built with three inverters as an example (two inverter systems are not further described). The effectiveness of the proposed control strategy is verified by comparing the conventional droop control, the adaptive virtual impedance control and the secondary voltage and frequency recovery control. The effectiveness of the control strategy proposed

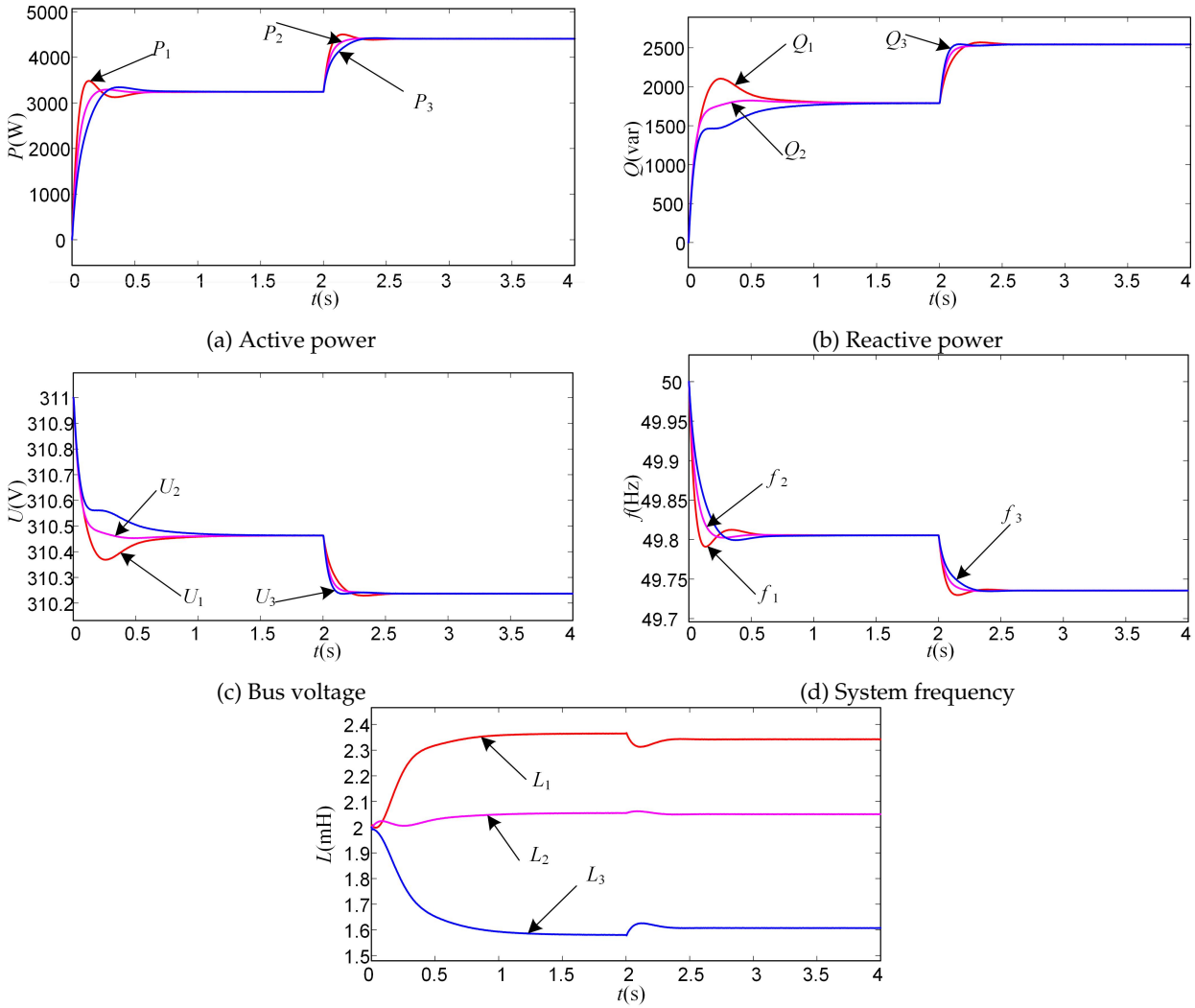

(a) Active power

(b) Reactive power

(c) Bus voltage

(d) System frequency

(e) Adaptive virtual impedance

Fig. 9. Adaptive virtual impedance simulation diagram

in this paper is verified. Among them, the action time is: 1 s before three parallel inverters supply power to load 1(12 kW + 6kvar); at 1 s, in order to verify the control effect of the real droop control, the load is simulated to be suddenly added and subtracted, and load 2(6 kW + 3kvar) is connected through the circuit breaker. At this time, the inverter provides energy for both loads together. The system simulation parameters are shown in Table 1.

Fig. 8 shows the simulation results of conventional droop control. Before and after the load surge, the active power is reasonably equalized when the system reaches the stable operation. However, at the same time, the system frequency decreases relative to the rated frequency. Due to the difference in line impedance of each DG output, the reactive power cannot be balanced in the conventional droop. And the reactive power output increases with the increase of line impedance, on the contrary, the bus voltage shows a small decreasing trend with the increase of line impedance.

Fig. 9 shows the graph of simulation results with the introduction of adaptive virtual impedance. Under the effect of the virtual impedance, the reactive power output is greatly improved compared to the conventional droop control when the system reaches the stable operation state. The reactive power output of each DG achieves a good equalization effect. The adaptive virtual impedance can be obtained to eliminate the difference between line impedances and achieve the reactive power equalization perfectly. And it can be seen from (e) that the value of adaptive virtual impedance is inversely proportional to the line impedance value.

Fig. 10 shows the secondary control simulation diagram at power equalization. The secondary control strategy is

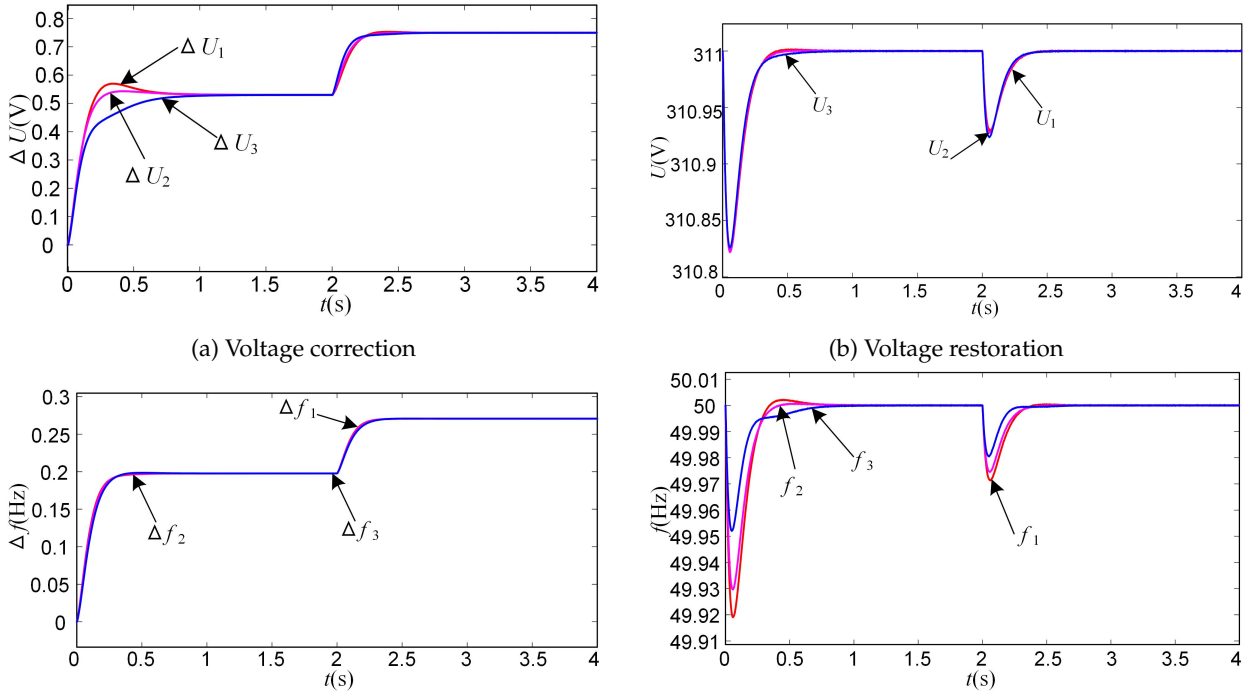

(a) Voltage correction

(b) Voltage restoration

(c) Frequency correction

(d) Frequency restoration

Fig. 10. Secondary recovery control simulation diagram

proposed for voltage and frequency reduction. Before and after load variation, when the system reaches steady state operation. The voltage and frequency correction terms are generated using the output voltage and frequency of each DG and fed back to the conventional droop control to achieve voltage and frequency recovery. The voltage is maintained at the rated voltage of 311V during stable operation, and the frequency is also restored to the rated value of 50HZ of the grid.

7. Conclusion

In this paper, the power distribution of microgrid under conventional droop control is analyzed as an example of low-voltage microgrid. And the conditions required for power equalization are derived. For the problem that the power cannot be reasonably divided equally due to different output line impedances. In this paper, an adaptive virtual impedance method is proposed to generate adaptive virtual impedance values through the power feedback of each DG, which compensates the differences between line impedances and achieves power equalization well. For the voltage and frequency offset problems caused by the traditional droop control and virtual impedance, this paper proposes a secondary control strategy for frequency and voltage recovery based on the traditional droop control. The correction terms generated by the output frequency and voltage are introduced in the conventional droop control, and the frequency and voltage values are well recovered. In the steady state operation, both voltage and frequency can be recovered to the rated value to improve the power quality of the microgrid. The simulation results show that the proposed adaptive virtual impedance and voltage and frequency secondary recovery control strategies are effective and feasible. The microgrid secondary control strategy based on adaptive virtual impedance proposed in this paper still has some deficiencies. The simulation study in this paper is under low voltage off-grid. Whether the strategy meets the requirements for the high-voltage grid or the seamless switching between the two modes of operation, grid-connected and off-grid, is not involved. This is also the focus of the next research work to be carried out.

8. Acknowledgments

This work was supported by the Natural Science Foundation of Gansu Province (23JRRA872) and the National Key Research and Development Plan Project of China (2017YFB1201003-20).

References

[1] S. K. Sharma, V. Gali, S. K. Gupta, et al., (2022) *"A Novel Hilbert Transform Weight-Factor Based Control*

Strategy For Grid Connected PV System With Multifunctional Capability" **Journal of Applied Science and Engineering *26***(9): 1263–1271. DOI: 10.6180/jase.202309_26(9).0007.

[2] J. Chen, Y. Zhou, X. Li, and Y. Tian, (2022) *"Research on hybrid energy storage control strategy of optical storage DC microgrid"* **Smart Power *50***(1): 14–20. DOI: 10.1007/s42835-022-01367-x.

[3] V. Gurugubelli, A. Ghosh, and A. K. Panda, (2022) *"Parallel inverter control using different conventional control methods and an improved virtual oscillator control method in a standalone microgrid"* **Protection and Control of Modern Power Systems *7***(1): 1–13. DOI: 10.1186/s41601-022-00248-9.

[4] C. Hu, Z. Cai, Y. Zhang, R. Yan, Y. Cai, and B. Cen, (2022) *"A soft actor-critic deep reinforcement learning method for multi-timescale coordinated operation of microgrids"* **Protection and Control of Modern Power Systems *7***(1): 1–10. DOI: 10.1186/s41601-022-00252-z.

[5] V. Mortezapour, S. Golshannavaz, E. Pouresmaeil, and A. Yazdaninejadi, (2022) *"A new hybrid control technique for operation of DC microgrid under islanded operating mode"* **Protection and Control of Modern Power Systems *7***(1): 42. DOI: 10.1186/s41601-022-00263-w.

[6] Y. Wang, J. Tang, J. Si, X. Xiao, P. Zhou, and J. Zhao, (2023) *"Power quality enhancement in islanded microgrids via closed-loop adaptive virtual impedance control"* **Protection and Control of Modern Power Systems *8***(1): 10. DOI: 10.1186/s41601-023-00284-z.

[7] H. Xiao, J. Huang, X. Chen, Y. Lin, and C. Wu, (2021) *"DC microgrid voltage control strategy based on dynamic load distribution"* **Electric Power Automation Equipment *41***(8):

[8] G. Zhou, Y. Zhao, H. Li, and Y. Li, (2023) *"Synchronous fixed-frequency microgrid power allocation based on improved droop control"* **Power Electronics Technology *57***(80-84):

[9] V. Gali, P. K. Jamwal, N. Gupta, B. C. Babu, and A. Kumar, (2023) *"An auto-tuned droop coefficient-based controller for microgrid system to enhance grid resilience during blackouts"* **Sustainable Energy Technologies and Assessments *57***: 103313. DOI: 10.1016/j.seta.2023.103313.

[10] S. Lu, T. Zhang, and Y. Chen, (2020) *"Research on the method of reducing the voltage frequency offset of parallel inverter with different capacities in microgrid"* **Journal of Power System and Automation *32***:

[11] J. Xue, X. Zhang, and G. Zhou, (2023) *"A virtual impedance-based adaptive sagging strategy for microgrids"* **China Test *49***(97-103+110):

[12] L. Tu, R. Zhu, and C. Hong, (2023) *"Secondary control strategy for microgrid with time-lag consistency based on switching topology"* **Electrical Automation *45***(71-74+78):

[13] V. Gali, P. K. Jamwal, N. Gupta, and A. Kumar, (2023) *"Multimode control strategy to improve the power quality and autonomy of PV-Wind-BESS based microgrid using harmonic frequency adaptive observer filter"* **Electric Power Systems Research *225***: 109786. DOI: 10.1016/j.epsr.2023.109786.

[14] J. Zhou, J. Zhang, D. Mao, X. Ge, J. Ye, and L. Fang, (2021) *"Distributed finite-time events trigger quadratic coordinated control of islanded microgrids"* **Electric Power Automation Equipment *41***(11):

[15] C. Luo, Y. Liu, Q. Luo, and J. Qin, (2022) *"Reactive power control strategy for low-voltage microgrid based on dynamic sag factor"* **Electric power construction *43***(1): 78–86.

[16] Y. Wang, J. Tu, Q. Chen, and C. Pan, (2023) *"Research on microgrid droop control based on virtual negative resistance"* **Journal of Hubei Normal University (Natural Science Edition) *43***(68-74):

[17] H. Liu, X. Zhao, G. Li, and L. Song, (2023) *"Research on photovoltaic DC microgrid based on improved adaptive segmented droop control"* **Renewable Energy *41***(1214-1221): DOI: 10.13941/j.cnki.21-1469/tk.2023.09.002.

[18] Y. Zhang, X. Qu, M. Tang, R. Yao, and W. Chen, (2021) *"Design of nonlinear droop control in DC microgrid for desired voltage regulation and current sharing accuracy"* **IEEE Journal on Emerging and Selected Topics in Circuits and Systems *11***(1): 168–175. DOI: 10.1109/JETCAS.2021.3049810.

[19] X. Zeng and X. Wang, (2023) *"Virtual impedance-based distributed reactive power allocation strategy for microgrids"* **Science Technology & Engineering *23***:

[20] H. Su, Z. Zhang, and S. Wang, (2023) *"Island microgrid power control system based on adaptive virtual impedance"* **Frontiers in Energy Research *10***: 974288. DOI: 10.3389/fenrg.2022.974288.

[21] M. Eskandari and L. Li, (2019) *"Microgrid operation improvement by adaptive virtual impedance"* **IET Renewable Power Generation *13***(2): 296–307. DOI: 10.1049/iet-rpg.2018.5303.

[22] M. H. Khan, S. A. Zulkifli, R. Jackson, E. Garba, and N. Zeb, (2022) *"Decentralized Adaptive-Virtual-Impedance-Based Predictive Power for Mismatched Feeders in Islanded Microgrids"* **International Journal of Energy Research *12***(2):

[23] Q. Zhang, Q. Yu, J. Wang, J. Li, and Y. Zhang, (2021) *"Improved droop control based on segmented virtual impedance"* **Journal of Power Systems and Automation *33***(87-93): DOI: 10.19635/j.cnki.csu-epsa.000637.

[24] H. Liang, C. Zheng, Y. Gao, and P. Li, (2017) *"Research on improved droop control strategy for microgrid"* **Chinese Journal of Electrical Engineering *37***(17): 4901–4910.

[25] H. Zhang, S. Kim, Q. Sun, and J. Zhou, (2017) *"Distributed Adaptive Virtual Impedance Control for Accurate Reactive Power Sharing Based on Consensus Control in Microgrids"* **IEEE Trans. Smart Grid *8***(4): 1749–1761. DOI: 10.1109/TSG.2015.2506760.